RESEARCH ARTICLE

Design of a smart wearable health monitoring device for the elderly based on time series prediction of multiple physiological parameters

Yanqun Wen[1, *], Ningxuan Hong[2]

[1]School of Art and Design, Sanming University, Sanming 365004, Fujian, China. [2]Faculty of Humanities and Arts, Macau University of Science and Technology, Macau, China.

Received: February 2, 2024; **accepted:** April 2, 2024.

With the increase of age, the physical function of the elderly gradually declines, and various chronic diseases such as hypertension and coronary heart disease also increase correspondingly. Hypertension is one of the most common health problems in the elderly. It not only affects the quality of life of the elderly, but also may lead to a series of serious complications. Therefore, real-time monitoring and effective prediction of blood pressure in the elderly is particularly important. To address this issue, this study developed a smart wearable health monitoring device based on time series prediction of multiple physiological parameters for the elderly, which employed sensors and Ethernet for real-time monitoring and recording of physiological parameters. The data was then analyzed through a long and short-term memory (LSTM) network to predict future trends of each parameter. The gadget demonstrated an average inaccuracy of 3 mmHg for systolic blood pressure and 4 mmHg for diastolic blood pressure taken in a relaxed state during basic functional accuracy testing. Under cognitive pressure, the diastolic and systolic blood pressure averages had an error rate of 3 mmHg and 2 mmHg, respectively. The average error between the heart rate measured by the health monitoring equipment and the real heart rate of the subjects was 4 bpm. Under cognitive stress, the average error between the measured heart rate and the subjects' real heart rate was 8 bpm. Under different pressure conditions, the difference between the blood oxygen saturation measured by the health monitoring equipment and the real value of the subjects was less than 1%. In the time series prediction test, the LSTM network-based prediction model converged at 168 iterations. By analyzing historical data, this model could accurately predict future trends of each physiological parameter. The model's convergence speed was better than the comparison model. In the training set, the study's proposed time-series prediction model achieved an average accuracy of 94.23% in predicting blood pressure values. Similarly, the average accuracy of the time-series prediction model proposed by the study was 91.61% in the test set. Notably, the accuracy outperformed comparison algorithms in both the training and test sets. Therefore, the health monitoring device proposed by the study exhibited potential for practical applications.

Keywords: aging; health monitoring; blood pressure; heart rate; blood oxygen saturation; prediction; long and short-term memory networks.

[*]**Corresponding author:** Yanqun Wen, School of Art and Design, Sanming University, Sanming 365004, Fujian, China. Email: wenyanqun2011@163.com.

Introduction

With the increasing size of the global elderly population, the health of older persons has become a major challenge for the global society. With the gradual decline of physiological function in old age, the elderly are more vulnerable to chronic diseases, sudden health problems, and reduced quality of life [1, 2]. Health monitoring and timely interventions for older people are

therefore essential to ensure that they enjoy their right to a healthy, active, and autonomous life.

Long short-term memory (LSTM) is widely used in different fields due to its ability to deal with long-term dependence problems well and its high scalability [3, 4]. Kesiman *et al*. developed an application capable of automatically transliterating Balinese palm leaf manuscripts into Roman letters and applied the LSTM model to the application [5]. To improve the operation quality of road network traffic and promote the sustainable development of urban road network planning, Mao *et al.* proposed a model based on PSO-LSTM to predict road traffic speed and overall dynamic time series, which could effectively predict road conditions in different regions [6]. Wei *et al*. proposed a wind speed prediction model based on LSTM, which could predict the wind speed in a specific time in the future according to the historical wind speed records of different regions and weather conditions [7]. Kim *et al*. proposed a time series prediction model based on LSTM. The experimental results showed that this model could accurately predict stock trends and weather conditions, and its prediction accuracy was better than the existing model [8]. Friedrich *et al*. used environmental sensors to monitor the health status of the target population and evaluated the monitoring results with real data sets. The results showed that the average data of motion sensor events had a great correlation with the standardized geriatric physical fitness evaluation criteria [9]. Santhanaraj *et al*. studied an auxiliary robot and system for elderly care, which could effectively help to improve the effect of existing elderly care auxiliary work [10]. Guo *et al*. designed a walking stick driven by ultra-low frequency human motion, which could help people with motor impairment including the elderly to improve their quality of life [11]. However, all those current technologies have different issues in data accuracy and reliability, privacy and security, user acceptance and usage habits, and medical regulation and standardization.

Health monitoring (HM) for the elderly needs to be not only real-time but more importantly predictive. To improve the effectiveness, timeliness, foresight, and convenience of health monitoring for the elderly, this study proposed a smart wearable health monitoring device for the elderly based on multi-physiological parameter time series prediction using LSTM to predict the relevant physiological parameter (P-P) and applied it to smart wearable devices. The device would help to improve the accurate judgment of the current health status of the elderly and the assessment of the future health status of the elderly to help the medical staff to intervene in advance and improve the quality of life of the elderly. The research not only promoted the innovation and development of health monitoring technology, but also provided new perspectives and methods for health management, disease prevention and medical research.

Materials and methods

Smart wearable health monitoring device architecture for the elderly

In the process of developing this smart wearable health monitoring device for the elderly, both knowledge and technology from multiple fields such as hardware design, software development, and data science were combined. The design and development of the equipment was not only based on formula calculations, but also on actual data collection, analysis, and model training. The hardware part mainly included wristband measuring terminal (Pro-720 smart health monitoring bracelet) (HealthTech Innovations Ltd., Shenzhen, Guangdong, China) and wireless sensor network (Smart Link WSN-500) (Smart Link Communications Inc., Shanghai, China). The design of the bracelet measuring terminal considered the habits and physiological characteristics of the elderly, ensuring that it could be comfortably worn on the wrist, and real-time and accurate monitoring of physiological parameters such as blood pressure, blood oxygen

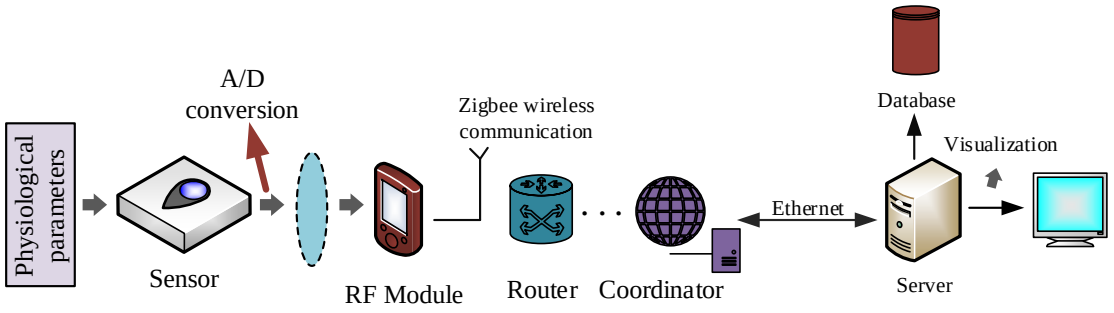

Figure 1. Framework diagram of intelligent wearable health monitoring equipment for the elderly.

saturation, and heart rate. The wireless sensor network was responsible for transmitting the data collected by the bracelet to the server and the monitoring center. The software part mainly involved the reception, processing, analysis, and visualization of data. A set of software specifically for processing physiological parameter data was developed to decode, store, and analyze the received data, and display and visualize it in real time in the monitoring center. During development, a large amount of data was used to train and validate the LSTM model to make predictions about physiological parameters of the elderly. Some of these data were collected from previous studies or publicly available databases, while others were collected through actual experiments. Blood pressure, oxygen saturation, and heart rate data were collected in a laboratory setting for 200 subjects between the ages of 60 and 80. This data was not only used to verify that the underlying function of the device was normal, but also to train and validate the LSTM model to improve the accuracy of the prediction. Each P-P was sent to the wireless sensor network through RF technology and was uploaded to the server and monitoring center through the coordinator in the wireless sensor network [12, 13]. The framework diagram of the smart wearable HM device for the elderly was shown in Figure 1. The real-time P-P monitored by the bracelet terminal was converted to a digital signal through the microprocessor built into the bracelet and an analog-to-digital converter, and sent to the wireless sensor network, and subsequently sent to the Dell PowerEdge R240 server (Dell (China) Co. Ltd., Beijing, China) using the ZigBee protocol (ZigBee) technology, which was a bi-directional wireless communication protocol with the advantages of low energy consumption and low data rate. Blood pressure, oxygen saturation, and heart rate were important P-P to determine the health status of the elderly. Measurement of blood pressure was generally done by direct and indirect methods, but direct measurement required invasive examination in hospitals or other specialized institutions, so it did not apply to this study. In this study, indirect measurement was used to collect blood pressure data from the wearers using pulse wave transit time (PWTT) and pulse wave velocity (PWV) methods [8, 14]. Equation (1) illustrated the link between the two methods and the blood pressure readings.

$$PWV = \frac{L}{PWTT} = \sqrt{\frac{hE}{\rho d}} = \sqrt{\frac{hE_0 e^{\alpha BP}}{\rho d}} \quad (1)$$

where L was the length of the artery. h was the thickness of the artery. ρ was the density of the blood. BP was the blood pressure. d was the diameter of the artery. α was the vascular parameter. E_0 was the elastic modulus at zero arterial pressure. As all other things being equal, when blood pressure increased, PWV rose, and conduction time decreased. The relationship between blood pressure and pulse conduction time was shown in equation (2).

$$BP = a * PWTT + b \quad (2)$$

where a and b were constants specific to the measurement object. The oximeter integrated within the bracelet allowed for the measurement of blood oxygen saturation. The oximeter emitted light of a specific wavelength. The oxygen saturation in the blood vessels was calculated using the different absorption responses of deoxyhemoglobin and oxyhemoglobin to specific wavelengths in equation (3).

$$I = I_0 \exp(-\varepsilon cL) \quad (3)$$

where I_0 was the light intensity of the incident light and I was the light intensity of the reflected light. ε was the absorption coefficient of the medium for the light. c was the concentration of the medium. L was the thickness of the medium. Since the pulse wave could reflect the beating frequency of the pulse, and at the same time, the beating frequency of the pulse was the same as the heart rate, the heart rate data could be obtained at the same time as the blood oxygen saturation of the wearer was measured [15, 16]. The wireless sensor network's tree network topology was depicted in Figure 2.

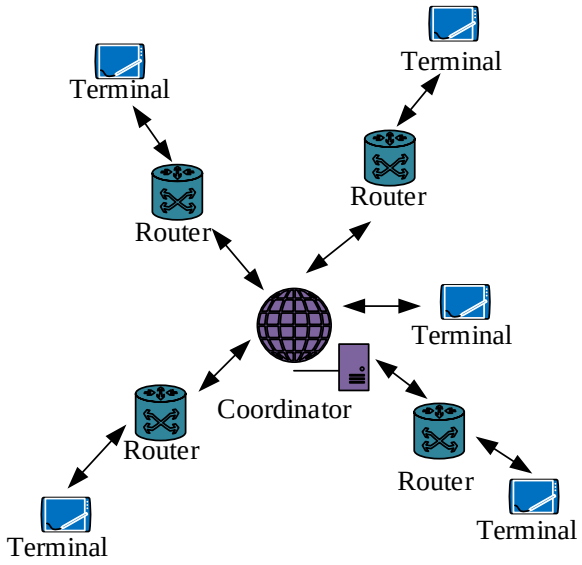

Figure 2. Tree topology of wireless sensor networks.

The wireless sensor network contained a coordinator, a variable number of routers, and terminals. The terminals could be sub-devices of either the router or the coordinator, but the end-devices had no sub-devices. The main function of the coordinator was to establish and maintain the network, and the main function of the router was P-P transit and routing. All data collected by the end devices would be transmitted to the coordinator, which uploaded it to the server *via* Ethernet. The server in the system mainly received the data frames sent by the coordinator and then decoded the data frames subsequently to obtain the P-P of the wearer and then stored each P-P into the database. The P-Ps were summarized and displayed in the monitoring center. The monitoring center consisted of software and hardware facilities. The software facility was mainly responsible for entering the wearer's information, binding the terminal device, monitoring the wearer's P-P in real time, and visualizing the P-P. The system set a threshold value for each P-P, and when a P-P exceeded the set threshold value, it would trigger a danger alert, which was convenient for the wearer or medical personnel to know the wearer's physical condition in time.

Predictive approach to multiple physiological parameters in the elderly

Time series forecasting is the forecasting of data related to time changes that are processed and analyzed. In HM systems, time series forecasting is done by modeling the historical data of P-P to predict the future trend of P-P. Depending on the forecast's step size, time series can be divided into single-step and multi-step forecasting categories [17]. The single-step forecasting, which involved using the subsequence in the known time period to predict the value of the sequence in the subsequent step, was expressed in Equation (4).

$$\hat{x}_{t+1} = \hat{f}(x_t \ldots x_{t-T+1}) \quad (4)$$

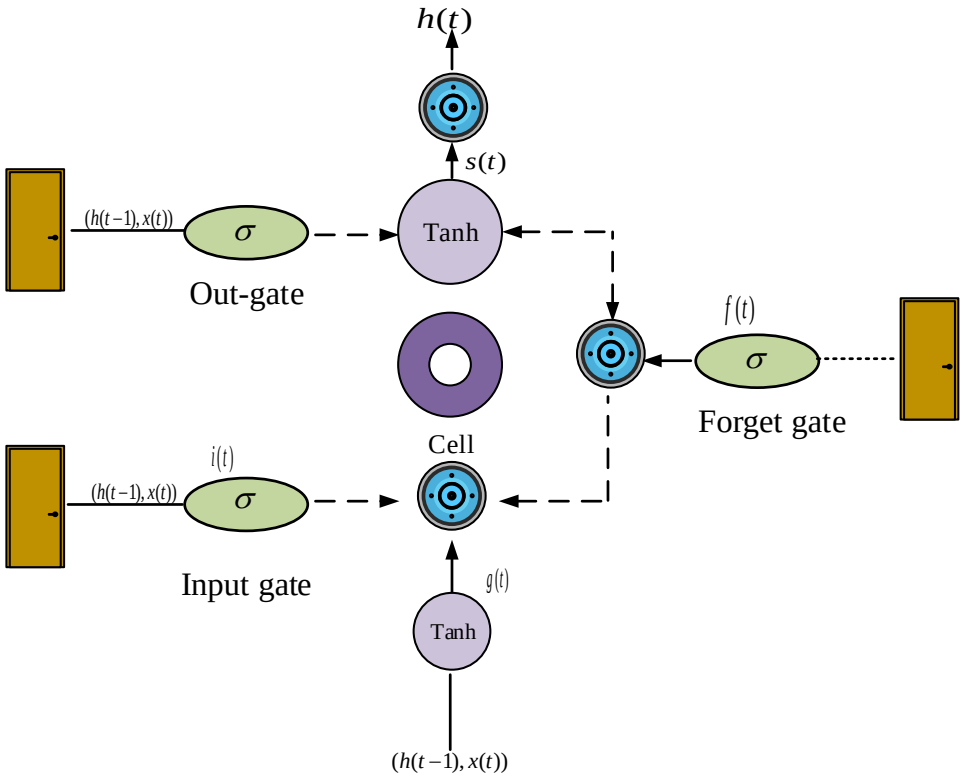

Figure 3. LSTM network structure diagram.

where $\hat{x}_{t+1}$ was the predicted value at the moment of $(t+1)$. $f(\cdot)$ was the relationship between the historical values of the time series and the future observations. Multi-step forecasting is generally applied to output by recursive forecasting or direct forecasting. Recursive prediction is output by minimizing the error of single-step prediction, and the result of single-step prediction is recursively used as model input, which in turn leads to the next multi-step prediction value. The recursive multi-step prediction expression was shown in equation (5).

$$\hat{x}_{N+k} = \begin{cases} \hat{f}(x_{N,\ldots,xN-T+Z}), k=1 \\ \hat{f}(\hat{x}_{N+k-1},\ldots,\hat{x}_{N+1},x_N,\ldots,x_{N-T+1}), 1<k\le T \\ \hat{f}(\hat{x}_{N+k-1},\ldots,\hat{x}_{N+k-T}), k>T \end{cases} \quad (5)$$

where $\left\{\hat{x}_{N+1},\hat{x}_{N+2},\ldots,\hat{x}_{N+K}\right\}$ was the output value of the model, i.e., the observations after k time steps that the model could predict. The single-step prediction method has a smaller error value compared to the multi-step prediction, so this study adopted the single-step prediction method for the elderly multi-P-P time series prediction. LSTM can lessen the issue of the recurrent neural network (RNN)'s long-term dependence and improve its long-term time series prediction performance. LSTM updates the recording time sequence of the cellular structure by the summation calculation, thus avoiding the large influence of the data of the previous state on this state data and retaining the time sequence of the cellular structure to avoid the large influence of the data of the previous state on this state data. Thus, it avoids the situation that the data of the previous state has a large influence on the data of this state and preserves the characteristics of the time step (Figure 3) [18,

19]. At moment t, the input layer input was $x(t)$. $h(t-1)$ was the hidden layer at moment $t-1$, and the internal state s was the secret key for neuron activation and determined the network structure of the LSTM. A value $f(t)$ between 0 and 1 was output through $h(t-1)$ and $x(t)$ in the internal state, representing a trade-off for fully retaining or discarding the state. The activation function was a sigmoid function. Equation (6) displayed the input gate equation.

$$i_t = \sigma\left(W_i \bullet x_t + U_i \bullet out_{t-1} + b_i\right) \quad (6)$$

where the input gate was represented by i_t. The information stored in the cell storing $h(t-1)$ and $x(t)$ were represented by W_i and U_i, respectively. The weight and bias of the input gate were represented by A. The output gate equation was shown below.

$$o_t = \sigma\left(W_o \bullet x_t + U_o \bullet out_{t-1} + b_o\right) \quad (7)$$

where X_t denoted the output data and $h(t-1)$ denoted the state at the previous moment. Typically, the output gate was determined by multiplying the memory cell state $s(t)$ result by the tanh activation function by a portion of the $h(t-1)$ and $x(t)$ result by the sigmoid activation function. The equation for the forgetting gate was shown in equation (8).

$$f_t = \sigma\left(W_f \bullet x_t + U_f \bullet out_{t-1} + b_f\right) \quad (8)$$

where $f(t)$ was the forgetting gate's output with W_f and U_f indicating the weight and bias of the forgetting gate, and W_o and U_o signifying the weight and bias of the output gate. The LSTM training algorithm utilized a backpropagation process, beginning with a forward propagation to obtain the neuron output value before subsequently calculating the value of the error in reverse. From there, the error function computed the partial derivatives of the neuron's weighted inputs *via* an equation, and the error equation was passed in a forward propagation to the previous state, which was expressed in Equation (9).

$$\delta_k^T = \prod_{j-k}^{t-1} \delta_0, {}^T_j W_{oh} + \delta_f, W_{fh} + \delta_i, {}^T_j W_{ih} + \delta_s, {}^T_j W_{sh} \quad (9)$$

where W_{xy} was the weight from cell x to cell y. $\delta_{f,J}$ was the error of the J th cell at moment f. $\delta_{i,J}$ was the error of the J th cell at moment i. $\delta_{s,J}$ was the error of the J th cell at moment s. The J error equation that propagated the error up one level was shown in equation (10).

$$\frac{\partial E}{\partial net_t^{l-1}} = (\delta_{o,t} {}^T W_{ox} + \delta_{f,t} {}^T W_{fx} + \delta_{i,t} {}^T W_{ix} + \delta_{s,t} {}^T W_{sx}) of'(net_t^{l-1}) \quad (10)$$

where W_{xy} was the weight from cell x to equation cell y. $\delta_{f,t}$ was the error of the t th cell at the f th moment. $\delta_{i,t}$ was the error of the t th cell at the i th moment. $\delta_{s,t}$ was the error of the t th unit at the s th moment. Recurrent convolutional neural network is a network model to deal with time-series data classification and regression problems after RNN. Its training speed is faster, and it can accurately control the dependencies in the time series. The three components of a recurrent convolutional neural network are the residual connection, the expansion convolution, and the causal convolution (Figure 4). The causal convolution is a unidirectional structure mainly used for processing temporal features. Equation (11) illustrated the causal convolution equation at point X_t in the current layer. The data of this layer was related to the values of the subsequent layer and its predecessors, but not to other moments of the present layer.

$$F * X\left(x_t\right) = \sum_{k=1}^{K} f_k x_{t-K+k} \quad (11)$$

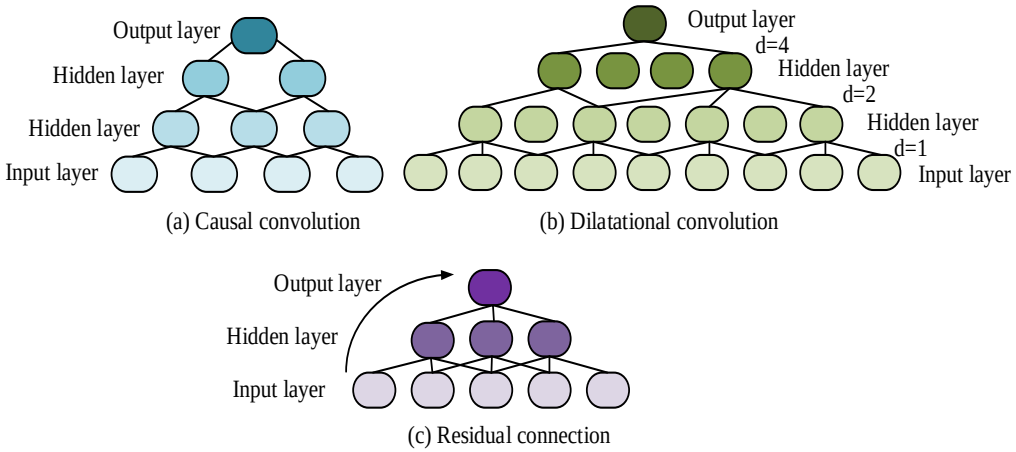

Figure 4. Recurrent convolutional neural network structure diagram.

where X was the sequence and F was the filter. The notion of expansion convolution was presented, and it was distinguished by the capacity to do interval time sampling, as causal convolution was restricted by the issue of the convolution kernel's size. The higher the interval d of the higher layer could make the convolution to expand the sensory field. The expansion convolution equation with expansion factor d at x_t was shown in equation (12).

$$F * X\left(x_t\right)=\sum_{k=1}^{K} f_k x_{t-(K-d)d} \tag{12}$$

where X was the sequence. F was the filter. d was the layer spacing. The residual connection could transfer information across the hidden layers and improve the problem of model accuracy degradation in deep learning. Over some time, the time series curve fluctuated, so before modeling the time series, it was necessary to test the smoothness of the time series. The study used the autocorrelation coefficient to analyze the relationship between the current time series monitoring values and the historical monitoring values. The expression of the autocorrelation coefficient was shown in equation (13).

$$\rho_T=\frac{Cov(X_t, X_{t-T})}{Var(X_t)} \tag{13}$$

where X_t was a subsequence of the time series corresponding to moment t. X_{t-T} was a subsequence of the time series at moment $t-T$. $Var(X_t)$ was the variance of X_t. $Cov(X_t, X_{t-T})$ was the self-covariance of X_t and X_{t-T}. The equation for the variance was then shown in equation (14).

$$Var(X_t)=\sum_{i=1}^{T}(X^i{}_t-\overline{X}_t)^2 \tag{14}$$

where $\overline{X}_t$ was the mean value of X_t. The equation for the self-covariance was as follows.

$$Cov(X_t, X_{t-T})=\sum_{i=1}^{T}(X^i{}_t-\overline{X}_t)(X^i{}_{t-T}-\overline{X}_{t-T}) \tag{15}$$

where $\overline{X}_{t-T}$ was the mean value of X_{t-T}. The user of the monitoring results judged the relationship between the data based on his/her own experience regarding the autocorrelation coefficient results to specify the appropriate monitoring strategy. The network of LSTM applied to multi-P-P time series prediction was shown in Figure 5. The LSTM network structure contained two layers with a cell count of 256, Layer L1 and Layer L2, and a fully connected layer

D1. The time steps were input into L1 in the order of $x_1, x_2 \ldots x_{t-1}, x_t$ with $h^{(1)}{}_{t-1}$ denoting the output of the $t-1$ time step of Layer L1. Subsequently, the output values of the L1 layer were input into the L2 layer for the same operation as L1. To simplify the model, only the hidden layer output $h^{(2)}{}_{T}$ of the L2 layer was returned. Finally, multiple P-P predictions of independent time steps were output by connecting to the fully connected layer D1 of 3 neurons.

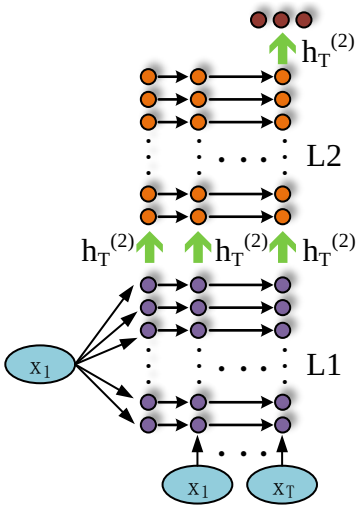

Figure 5. Schematic diagram of LSTM application in multiple physiological parameter time series prediction.

Testing of developed device

The basic and predictive features of this HM device were tested on a desktop computer with Inter(R) Core™ i5-13400U, operating system Windows 10, and 8 G of RAM. The study collected blood pressure, oxygen saturation, and heart rate data from 200 subjects in different physical states in a laboratory setting using Yuyue YE660AR arm-type electronic sphygmomanometer for blood pressure and heart rate and Omron HPO-100 oximeter for oxygen saturation, which was considered to be the genuine oxygen saturation. The subjects were 100 men and 100 women, aged 60-80 years old. Elderly people with relatively good health and able to cooperate with the experimental task were selected. All participants had no serious chronic diseases or disabilities and were able to maintain a stable physical state during the experiment. In addition, to ensure the reliability and validity of the data, participants who had severe cognitive impairments or were unable to properly understand and perform the requirements of the experiment were excluded. The procedures of this study were approved by the National Health Research Ethics Board for the use of human subjects/data. A consent form was signed by all participants before formally participating in the experiment. The study achieved different mental stress states by putting the experimental subjects in different environments. The relaxation state was achieved by allowing subjects to listen to music. The physical stress state was achieved by letting the subjects walk or jog. The emotional stress was achieved by letting the subjects watch movies with high emotional fluctuations. The cognitive stress was achieved by having the subjects read academic articles. All data was collected in a 20-minute duration.

Results and discussion

Basic functional accuracy testing

The blood pressure values measured with the different devices in a relaxed state showed that the average error between the diastolic blood pressure measured by the proposed HM device of this study and the true diastolic blood pressure value measured by the Yuyue YE660AR arm-type electronic sphygmomanometer was 4 mmHg, while the average error value of systolic blood pressure was 3 mmHg (Figure 6a). The average error between the diastolic blood pressure measured by HM and the real diastolic blood pressure value of the subjects in a cognitive stress state was 3 mmHg, while the average error of systolic blood pressure was 2 mmHg (Figure 6b). The error values in both relaxed and cognitive stress states satisfied the criteria of Association for the Advancement of Medical Instrumentation (AAMI) for the practical application. The results indicated that the blood

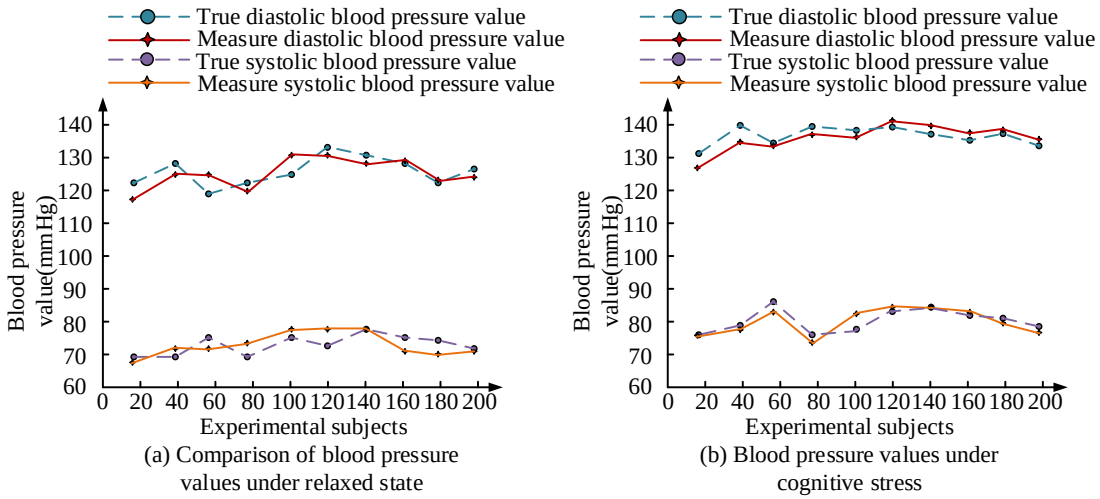

Figure 6. Comparison of blood pressure values.

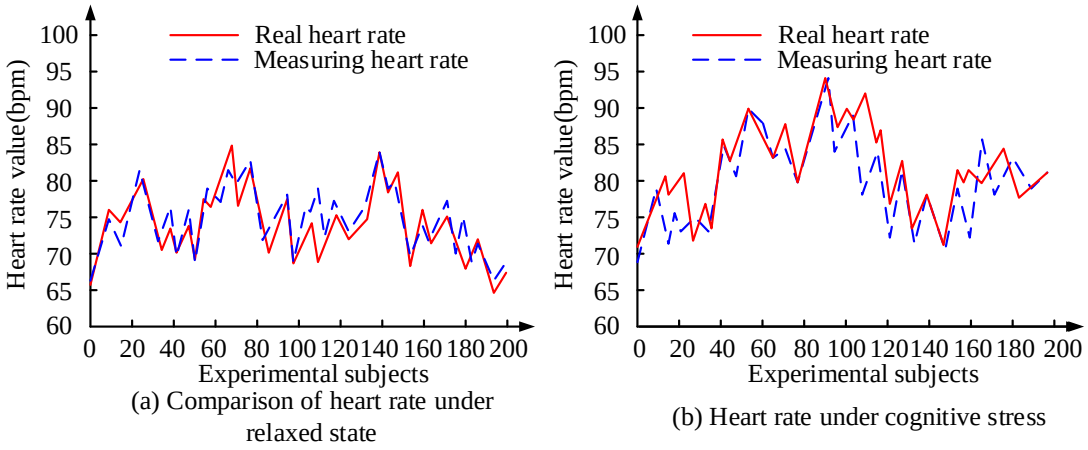

Figure 7. Comparison of heart rate values.

pressure values measured by the designed HM devices had a reference value. The average error of the heart rate between the HM device and the true heart rate of the subjects was 4 bpm under relaxed state (Figure 7a), while the average error of heart rate in cognitive stress state between the HM and the subject's true heart rate was 8 bpm (Figure 7b). The error value was lower in the relaxed state than that in cognitive stress state, which indicated that the heart rate measured by the HM device had a reference value. The blood oxygen saturation data measured in the relaxed state showed that the average error between the HM devices and the true values was 0.3% (Figure 8a), while, under body pressure, the average error between the HM and the true values was 0.8% (Figure 8b). The blood oxygen saturation data measured by different devices during the emotional stress state were shown in Figure 8c. The mean error between the oxygen saturation values measured by the HM device and the true values was 0.4%. The blood oxygen saturation data obtained from several devices during a cognitively stressed state was shown in Figure 8d. The oxygen saturation values measured by the HM device had a mean inaccuracy of 0.5% compared to the true values. The results showed less than 1% separation among the genuine

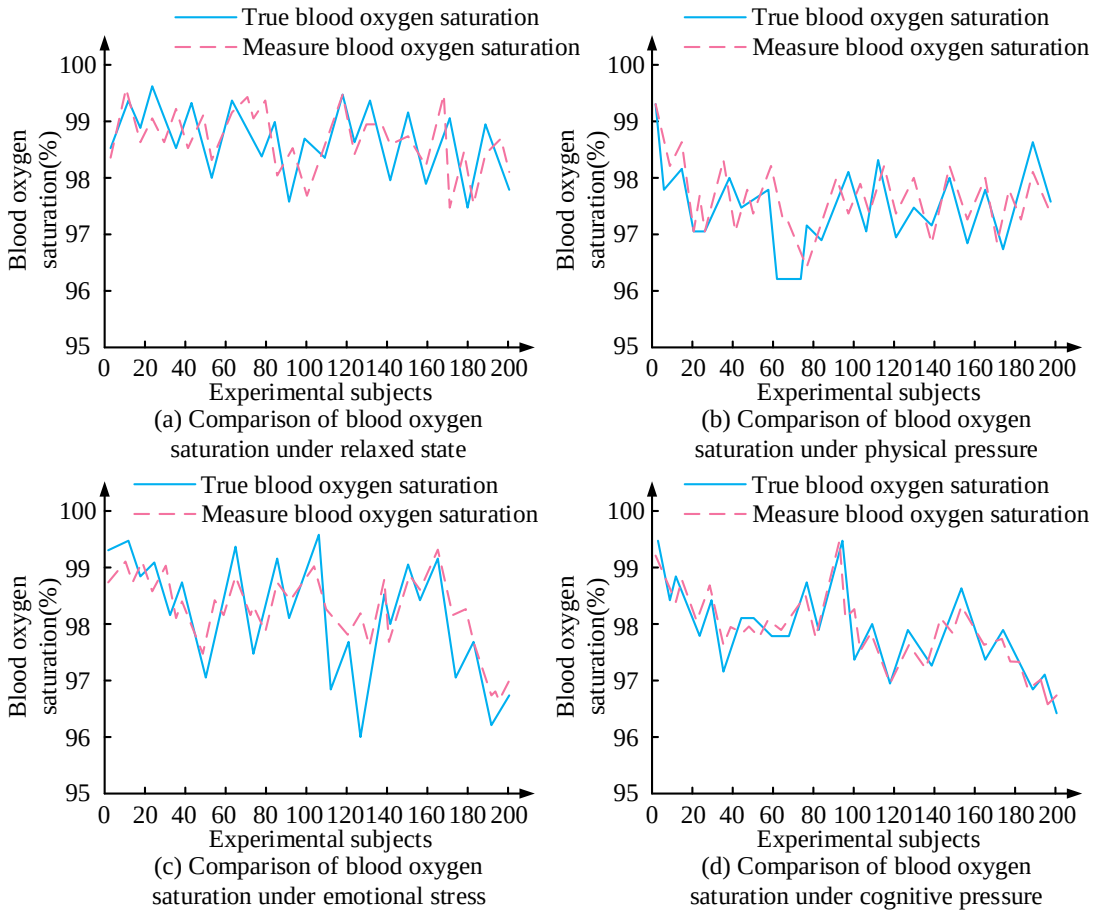

Figure 8. Comparison results of blood oxygen saturation values.

values of the participants under various stress conditions from the oxygen saturation values measured by the HM device, suggesting that the oxygen saturation recorded by the designed HM device had a reference value.

Time series forecasting functionality testing

The convergence performance of the prediction model developed in this study was compared to prediction models based on recurrent neural networks (RNN) and convolutional neural networks (CNN). The temporal prediction model based on LSTM, RNN, and CNN converged when the number of iterations reached 168, 235, and 326, respectively (Figure 9a). The time-series prediction model based on LSTM, RNN, and CNN completed convergence when the number of iterations reaches 251, 300, and 385, respectively (Figure 9b). A comparison of the blood pressure value prediction models' accuracy using various methods in the training dataset and test set was shown in Figure 10. Based on the calculations, the average accuracy of the temporal prediction model based on LSTM, RNN, and CNN were 94.23%, 89.51%, and 85.59%, respectively in training data set (Figure 10a). It was evident that the LSTM-based temporal prediction model exhibited strong stability in the measurement of blood pressure values, and its accuracy grew as the number of experimental subjects increased. The average accuracy of the temporal prediction model based on LSTM, RNN, and CNN in the test data set were 91.61%, 85.62%, and 82.13%, respectively (Figure 10b). In both the training and test sets, the suggested LSTM-based temporal prediction model for blood pressure prediction demonstrated a greater average accuracy than the comparison models. The study chose mean

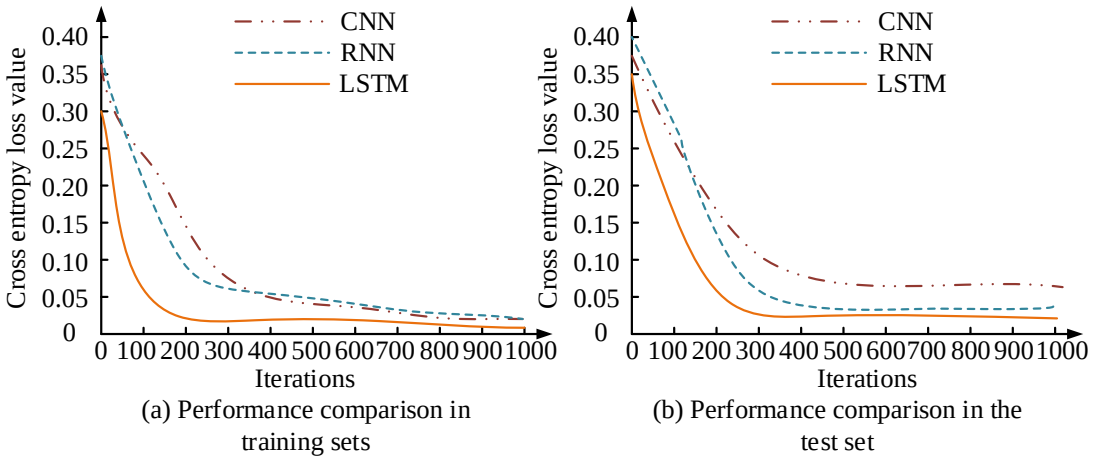

Figure 9. Comparison of convergence performance of different algorithms in different datasets.

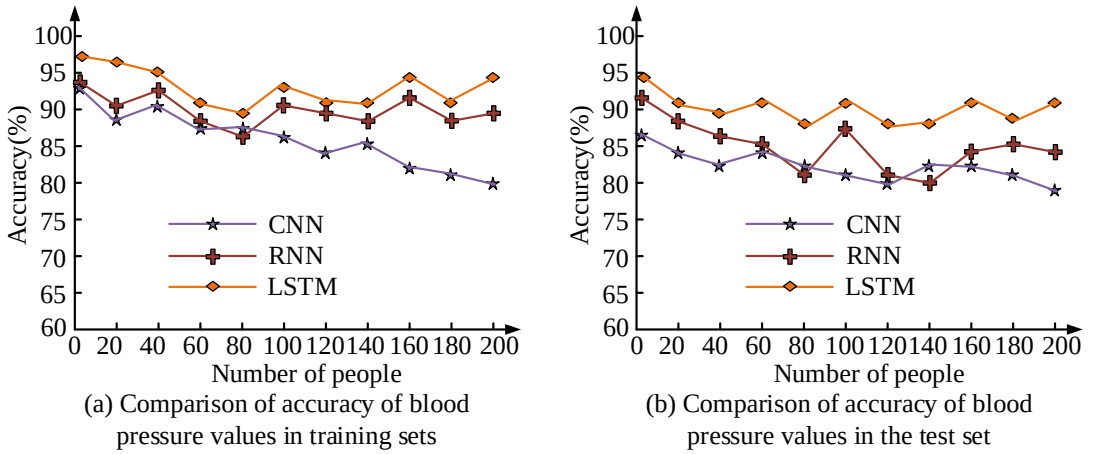

Figure 10. Comparison of time series prediction accuracy of blood pressure values.

Table 1. The mean value of performance indicators of different evaluation methods.

Performance evaluation index	LSTM	RNN	CNN
MRE	8.56%	10.23%	15.68%
MSE	9.15%	13.33%	16.75%
MAE	8.68%	11.32%	14.26%
RMSE	0.1947	0.3869	0.5391

square error (MSE), root mean square error (RMSE), mean absolute error (MAE), and mean square error (MRE) as the evaluation metrics for various prediction models in order to guarantee the test's accuracy. The results showed that the LSTM model outperformed other models in terms of evaluation metrics with MRE, MSE, MAE, and RMSE as 8.56%, 9.15%, 8.68%, and 0.1947, respectively (Table 1), indicating its superior performance. These results showed that the time series prediction model based on LSTM had good predictive power.

Conclusion

Addressing issues with non-portable HM devices for the elderly and the unpredictability of P-P in this population, this study developed a smart wearable HM device based on MPPTSP. The device was subject to a basic accuracy test, resulting in an average error of 4 bpm between measured and true heart rate in a relaxed state. The average error for heart rate measurements under cognitive stress was 8 bpm. The LSTM model achieved an MRE of 8.56%, MSE of 9.15%, MAE of 8.68%, and RMSE of 0.1947 during evaluation. The results revealed that the HM device, which took MPPTSP into account, had a strong detection ability and could report the wearer's health in real-time. Additionally, the comparative analysis demonstrated the utility of the Institute's HM device for the elderly, which could be attributed to the familiarity of commonly used devices in the market. However, this study did not measure the P-P movement, which also resulted in increased requirements for the device's monitoring environment. Therefore, future research should aim to enhance the device's intelligent detection ability by incorporating movement detection technology, which will provide real-time HM to elderly individuals while in motion and contribute to their overall wellbeing.

Acknowledgement

The research was supported by the Social Science Fund Project of Fujian Province, China (Grant No. FJ2023X010).

References

1. Obeidat Y, Alqudah A. 2021. A hybrid lightweight 1D CNN-LSTM architecture for automated ECG beat-wise classification. J Biomed Eng. 38(5):1281-1291.
2. Zhu Z, Zhu X, Cai Y, Zhu H. 2021. Large-scale terminal access algorithm based on slot ALOHA and adaptive access class barring. Chinese J Internet Things. 5(1):90-98.
3. Ztürk MM. 2023. Hyperparameter optimization of a parallelized LSTM for time series prediction. Vietnam J Comput Sci. 10(03):303-328.
4. Latif SD, Ahmed AN. 2021. Application of deep learning method for daily streamflow time-series prediction: A case study of the Kowmung River at Cedar Ford, Australia. Int J Sustainable Dev Planning. 16(3):497-501.
5. Kesiman MWA, Dermawan KT. 2021. AKSALont: Automatic transliteration application for Balinese palm leaf manuscripts with LSTM Model. J Teknologi dan Sistem Komputer. 9(3):142-149.
6. Mao Y, Qin G, Ni P, Liu Q. 2021. Analysis of road traffic speed in Kunming plateau mountains: a fusion PSO-LSTM algorithm. Int J Urban Sci. 26(1):87-107.
7. Wei CC. 2021. Collapse warning system using LSTM neural networks for construction disaster prevention in extreme wind weather. J Civil Eng Management. 27(4):230-245.
8. Kim EB, Park JH, Lee YS, Lim C. 2021. Two-dimensional attention-based multi-input LSTM for time series prediction. Commun Stat Appl Metho. 28(1):39-57.
9. Friedrich B, Steen EE, Fudickar S, Hein A. 2021. Analyzing the correlation of geriatric assessment scores and activity in smart homes. Int J UbiComp. 12(2):1-15.
10. Santhanaraj KK, Ramya MM, Dinakaran D. 2021. A survey of assistive robots and systems for elderly care. J Enabl Technol. 15(1):66-72.
11. Guo X, He T, Zhang Z, Luo A, Lee C. 2021. Artificial intelligence-enabled caregiving walking stick powered by ultra-low-frequency human motion. ACS Nano. 15(12):19054-19069.
12. Karl Y. 2021. Big data management system for U-healthcare. Int J Software Innovation. 9(1):1-11.
13. Kota VR, Munisamy SD. 2022. High accuracy offering attention mechanisms based deep learning approach using CNN/bi-LSTM for sentiment analysis. Int J Intel Comput Cybernetics. 15(1):61-74.
14. Xiao Y, Yin H, Zhang Y, Qi H, Liu Z. 2021. A dual-stage attention-based Conv-LSTM network for spatio-temporal correlation and multivariate time series prediction. Int J Intelligent Systems. 36(5):2036-2057.
15. Kumar P, Hariharan K. 2022. Time series traffic flow prediction with hyper-parameter optimized ARIMA models for intelligent transportation system. J Sci Indust Res. 81(4):408-415.
16. Guo Y, Mustafaoglu Z, Koundal D. 2022. Spam detection using bidirectional transformers and machine learning classifier algorithms. J Comput Cognit Engin. 2(1):5-9.
17. Yang Y, Song X. 2022. Research on face intelligent perception technology integrating deep learning under different illumination intensities. J Comput Cognit Engin. 1(1):32-36.
18. Hanif R, Mustafa S, Iqbal S. 2023. A study of time series forecasting enrollments using fuzzy interval partitioning method. J Comput Cognit Engin. 2(2):143-149.
19. Al-Mejibli I, Al-Majeed S, Karam J, Iqbal J. 2021. System architecture of a proactive intelligent system to monitor health of older adults living alone. IJCDS J. 10(1):509-517.